Urban Climate 51 (2023) 101615

Contents lists available at ScienceDirect

Urban Climate

journal homepage: www.elsevier.com/locate/uclim

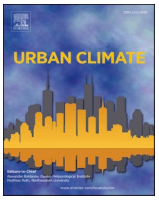

Comparing land surface temperature and mean radiant temperature for urban heat mapping in Philadelphia

Xiaojiang Li [a,*], TC Chakraborty [b], Guoqing Wang [c,d,e]

[a] Department of Geography and Urban Studies, Temple University, Philadelphia, PA, United States
[b] Atmospheric Sciences & Global Change Division, Pacific Northwest National Laboratory, Richland, WA, USA
[c] Biometeors, LLC, PA, USA
[d] NASA Goddard Space Flight Center, Greenbelt, MD 20771, USA
[e] Science Systems and Applications, Inc. (SSAI), Lanham, MD 20706, USA

ARTICLE INFO

Keywords:
Urban heat metrics
Land surface temperature
Mean radiant temperature
SOLWEIG model

ABSTRACT

Many cities are experiencing more frequent extreme heat during hot summers. With the rise of global temperature, the thermal comfort in urban areas become even worse. Quantitative information of the spatial distributions of urban heat has become increasingly important for resilience and adaptation to climate change in cities. This study compares satellite-derived land surface temperature (LST) and urban microclimate modeling-based mean radiant temperature (Tmrt) for mapping the urban heat distributions in Philadelphia, Pennsylvania, USA.

The LST was estimated based on Landsat 8 thermal imagery with a spatial resolution of around 100 m, while the Tmrt was simulated based on high resolution LiDAR and national aerial imagery program multispectral aerial imageries with a spatial resolution of 1 m. Result shows that both LST and Tmrt show a similar general pattern of the urban heat across the study area, while the Tmrt presents much more details of the heat variations street by street and neighborhood by neighborhood. The LST tends to have a stronger relationship with the Tmrt on building roofs, which are usually not the place for human activities. This studyprovides evidence for choosing more appropriate metrics in urban heat-related studies.

1. Introduction

Extreme heat events have increasingly become a severe threat to public health, particularly in heavily populated urban areas, due to both global warming and rapid urbanization (Lin et al., 2012; Luber and McGeehin, 2008; Watts et al., 2015). The frequency of these events is increasing in large U.S. cities, and, on average, they are responsible for a greater number of climate-related annual fatalities than any other forms of extreme weather (Stone et al., 2010; Borden and Cutter, 2008). There is evidence showing increases in mortality in cities during heat waves, with implications for future climate (Laaidi et al., 2012; Gabriel and Endlicher, 2011). Moreover, ambient heat stress can deteriorate livability and walkability in cities (Lee et al., 2013).

A quantitative understanding of the heat distributions in cities is important for monitoring vulnerability and building resilience, particularly for adaptation to climate change (Li, 2021; Hsu et al., 2021; Reid et al., 2009). Air temperature is a critical factor for human heat risk and has been widely used to understand human heat stress's relation to public health (Noelke et al., 2016; Ho and

* Corresponding author.
E-mail address: lixiaojiang.gis@gmail.com (X. Li).

https://doi.org/10.1016/j.uclim.2023.101615
Received 16 November 2022; Received in revised form 14 July 2023; Accepted 16 July 2023
Available online 29 July 2023

Wong, 2019; Wang et al., 2018). Nevertheless, air temperature is typically measured at a limited number of fixed weather stations, which hinders its ability to accurately represent the spatial variations of air temperature within cities. Comparatively, satellite-derived land surface temperature (LST) offers an efficient method to map the spatial distributions of urban heat across scales. Previous studies have reported a weak correlation between LST and ambient air temperature, though a stronger relationship was observed during nighttime (Cao et al., 2021; Mutiibwa et al., 2015; Vancutsem et al., 2010; Venter et al., 2021; Zhang et al., 2014). Therefore, LST has been used to estimate the spatial distribution of nighttime air temperature (Mutiibwa et al., 2015; Vancutsem et al., 2010; Zhu et al., 2013). LST has also been widely used in urban heat-related studies with the assumption that it serves as a reasonable proxy for quantifying urban heat exposure (Chen et al., 2006; Harlan et al., 2013; Jenerette et al., 2016; Pearsall, 2017; Chakraborty et al., 2019; Hsu et al., 2021) and has been employed in conjunction with other socio-economic factors to develop heat vulnerability indices (Reid et al., 2009; Hammer et al., 2020; Weber et al., 2015). However, satellite-derived LST cannot comprehensively capture human heat stress on the ground, since human heat stress is influenced by ambient temperature, radiation, humidity, and many other factors (Norton et al., 2015; Klemm et al., 2015; Li and Wang, 2021; Li, 2021; Chakraborty et al., 2022). Moreover, coarse-resolution satellite imagery cannot resolve the shade of trees and building blocks (Yu et al., 2020).

An important and understudied aspect of heat exposure in cities is solar radiation. A person directly exposed to solar radiation gets significantly more heat exposure than someone staying in the shade. However, LST, air temperature, and many commonly used metrics of moist heat stress do not account for solar radiation. Fine scale microclimate modeling based on high-resolution, three-dimensional urban models and local meteorological data provides a more comprehensive way to model the dynamically changing urban thermal environment (Lindberg et al., 2008; Lindberg et al., 2018; Lindberg and Grimmond, 2011; Li, 2021; Li and Wang, 2021; Matzarakis et al., 2007, 2010; Maronga et al., 2015). By simulating the solar radiation reaching the ground, it is possible to compute the mean radiant temperature (T_{mrt}), which is the total net short and longwave radiation that a human is exposed to from the surrounding environment. It plays a significant role in influencing the human energy balance (Ali-Toudert and Mayer, 2006; Matzarakis et al., 2010; Mayer and Höppe, 1987; Thorsson et al., 2014; Vanos et al., 2012; Aviv et al., 2021; Middel and Krayenhoff, 2019). A strong correlation has been observed between T_{mrt} and heat-related mortalities (Thorsson et al., 2014). However, there are only a few studies that use T_{mrt} for city-scale analyses (Kong et al., 2022; Li, 2021; Li and Wang, 2021; Kianmehr et al., 2023). The reason for this limitation stems from the substantial computational costs associated with conducting radiation simulations based on high resolution urban 3D models. Recently developed GPU-accelerated algorithms for urban microclimate modeling can efficiently generate T_{mrt} with high spatio-temporal resolution at large scales (Li and Wang, 2021). As high-resolution urban 3D models become more widely accessible for numerous cities, T_{mrt} is emerging as a new promising heat exposure metric for conducting urban-scale heat-related studies.

In this study, computed fine-resolution T_{mrt} from 3D models was compared with medium-resolution LST obtained from Landsat imagery to create urban heat maps for the city of Philadelphia in the United States. The findings of this analysis offer valuable insights for selecting more appropriate heat exposure metrics to investigate urban heat and its intra-urban variability.

2. Methodology

2.1. Study area and data preparation

Our study area is the city of Philadelphia in the United States (Fig. 1). The datasets used in this study include a high resolution (1 m)

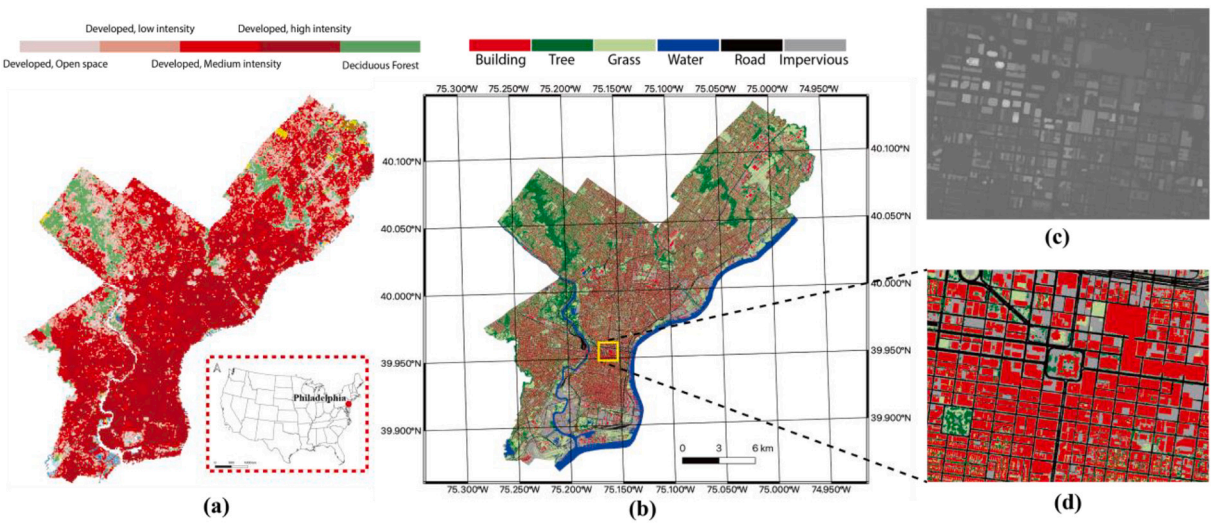

Fig. 1. The location and datasets used in the study area, (a) the National Land Cover Dataset for Philadelphia, (b) the fine level resolution land use data in Philadelphia, (c) the normalized digital surface model of the downtown Philadelphia, and (d) the land use map in the downtown of the Philadelphia.

land use map, LiDAR cloud point data, medium resolution Landsat 8 thermal imagery, National Land Cover Dataset (NLCD), and meteorological data from National Renewable Energy Laboratory (NREL) (Fig. 1). The high-resolution land use map was created semi-automatically based on high-resolution aerial imageries and LiDAR data with accuracy as high as 90% by Urban Tree Canopy Project from University of Vermont. The high-resolution LiDAR data are in the form of pre-processed x, y, z points cloud files from United States Geological Survey 3D Elevation Program (https://usgs.entwine.io/). In this study, the open-sourced tool Point Data Abstraction Library (PDAL) was used to convert the LiDAR cloud points into digital elevation model (DEM) and digital surface model (DSM) automatically. The high-resolution land use map and the generated DSM were combined to generate the building height model and the tree canopy height model. In addition, the NLCD data of 2019 with the spatial resolution of 30 m and the Landsat 8 thermal imageries with the spatial resolution of ~100 m in the summer of 2019 were also collected for the study area. The meteorological data in 2019 was collected from NREL (https://nsrdb.nrel.gov/). The meteorological data include the hourly global horizontal radiation, direct radiation, diffuse radiation, relative humidity, etc.

2.2. Land surface temperature mapping

In this study, the land surface temperature (LST) was calculated for each approximately 100-m pixel from all available cloud-free Landsat 8 Collection 2 images captured during the northern hemisphere summer months (June, July, August) in 2019 over the city of Philadelphia. This LST was derived from top of the atmosphere thermal infrared radiation between 10.60 and 11.19 μm measured by Landsat after taking into consideration land surface properties (emissivity, vegetation cover, etc.) and atmospheric auxiliary data (Hulley et al., 2015). The summertime composites were for June 2nd, July 4th, July 20th, August 5th, and August 21st, 2019, with an overpass time around 11:30 am local time. Pixel-level quality control flags were applied to the observations to identify and exclude areas affected by cloud contamination. The cloud-free Landsat image captured on July 20, 2019 was further used in comparison of LST with the corresponding T_{mrt}. Due to the method of observation, the LST represents a directional measure of the radiative temperature of all objects viewed by Landsat and, it is also somewhat sensitive to the retrieval algorithms used (Sekertekin and Bonafoni, 2020) and the method for specifying surface emissivity (Chakraborty et al., 2021).

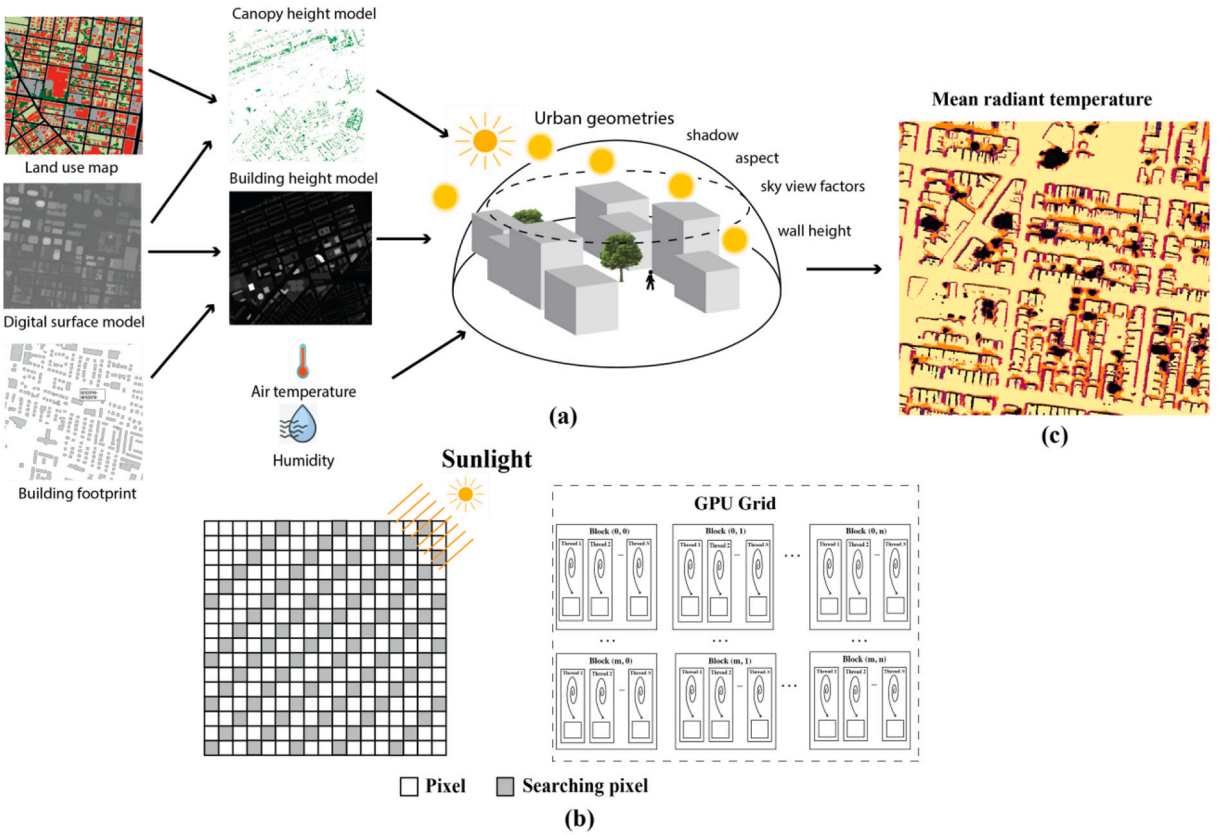

Fig. 2. The calculation of the mean radiant temperature (T_{mrt}) using the SOLWEIG model based on high resolution land use map, digital surface model, building footprint map, and meteorological data using the GPU-accelerated algorithm, (a) the SOLWEIG model for computing the T_{mrt}, (b) the GPU-accelerated algorithm, (c) the spatial distribution of the computed T_{mrt} in part of the study area.

2.3. Mean radiant temperature estimation

The mean radiant temperature (T_{mrt}) is the integrated net shortwave and longwave radiation that human body is exposed to from the surrounding environment and the T_{mrt} is the most significant meteorological input parameter for human energy balance, especially on clear and calm summer days (Mayer and Höppe, 1987). In urban areas, solar radiation undergoes various processes including reflection, absorption, and re-reflection by vertical urban surfaces. A portion of this radiation is trapped within street canyons and re-emitted as longwave radiation. Obstructions, such as buildings and trees, act as barriers that block the solar radiation, thereby further reducing the amount of solar radiation reaching the street canyons. In this study, the SOlar and LongWave Environmental Irradiance Geometry model (SOLWEIG) was used to calculate T_{mrt} (Thorsson et al., 2014; Lindberg and Grimmond, 2011; Lindberg et al., 2008) based on high resolution building height model, tree canopy height model, together with radiation, air temperature, and air humidity collected from local weather stations as inputs (Fig. 2). The SOLWEIG is a three-dimensional solar radiation model designed to estimate the fluctuations of shortwave and longwave radiation fluxes. This model considers shadow patterns and the reflection and absorption of solar radiation by geometrical characteristics of buildings and trees. The SOLWEIG model has been validated worldwide in different climate zones with high accuracy (Chen et al., 2016; Lindberg and Grimmond, 2011; Gál and Kántor, 2020; Buo et al., 2023). In

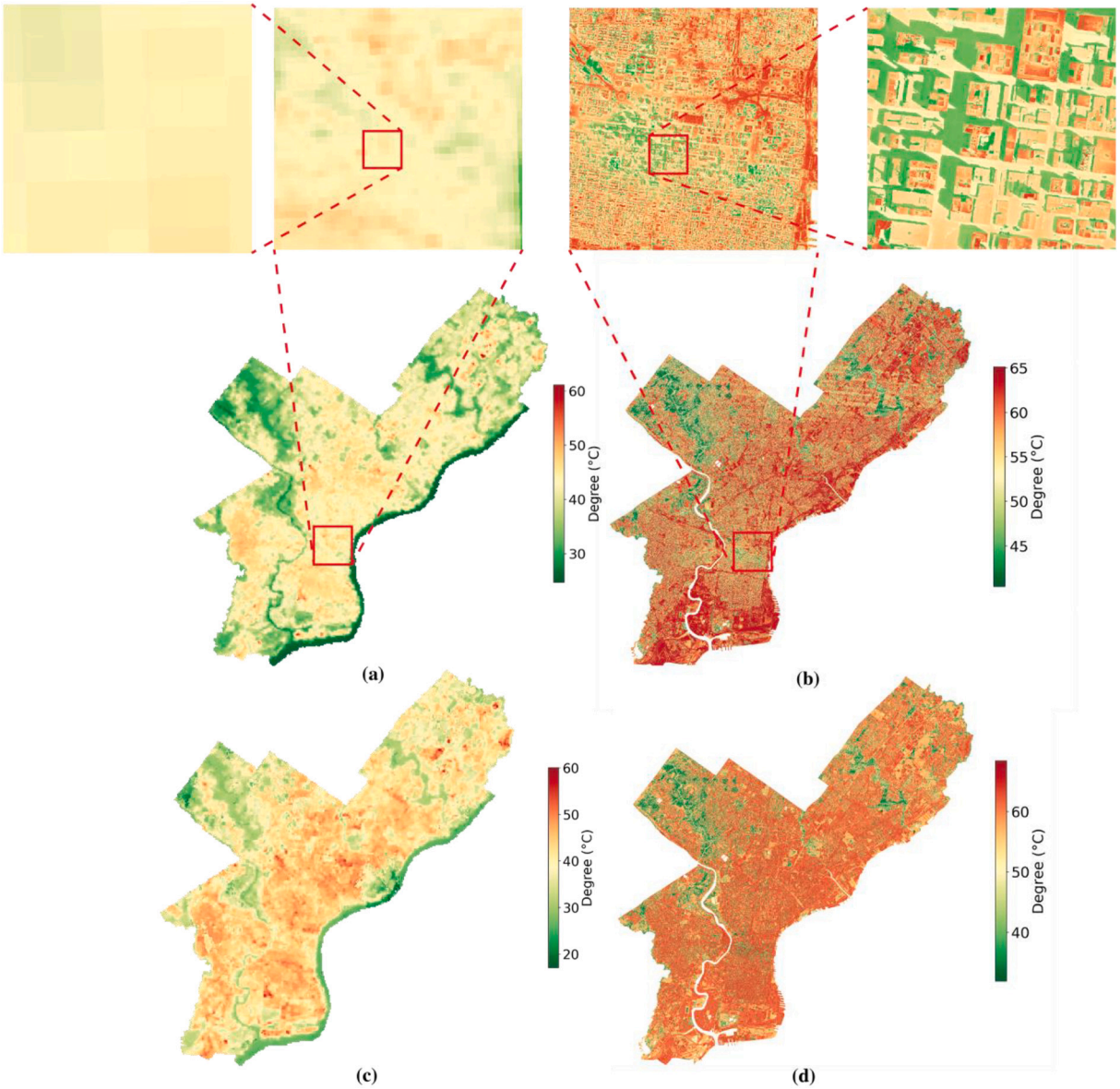

Fig. 3. The spatial distributions of the land surface temperature (LST) on July 20th, 2019 at 11:30 am local time (a), the mean radiant temperature (T_{mrt}) on July 20th, 2019 at 11:30 am (b), the averaged LST in summer of 2019 (c), and the averaged T_{mrt} at the same periods of LST (d).

SOLWEIG model, the T_{mrt} can be calculated as (Lindberg et al., 2008; Lindberg and Grimmond, 2011),

$$T_{mrt} = \sqrt[4]{R/\varepsilon_p \sigma} - 273.15 \quad (1)$$

where σ is the Boltzmann constant, ε_p is the emissivity of the human body, and R is the radiation that a human body exposed and can be estimated as,

$$R = \xi_k \sum_1^6 K_i F_i + \varepsilon_p \sum_1^6 L_i F_i \quad (2)$$

where K_i is the shortwave radiation component from 6 directions (north, south, west, east, top, and bottom), L_i is the longwave radiation, F_i is the angular factor between a person and the surrounding environment, ξ_k is the absorption coefficient for shortwave radiation (standard value 0.7), ε_p is the emissivity of the human body (standard value 0.97) (Fig. 2(a)). The SOLWEIG model is computationally expensive when running on CPUs at fine resolutions (Li, 2021; Li and Wang, 2021). This study adopted the previously developed GPU-based method to accelerate the SOLWEIG model (Li and Wang, 2021). The NVIDIA computing framework PyCUDA was used in this study to combine the Python and C programming languages for pixel-level computation. The Python was used to handle the spatial information of pixels, and the C was used to conduct massive pixel-level operations for modeling the radiation on GPU in parallel. Fig. 2(b) shows the computational model of the GPU-accelerated model for computing the T_{mrt} based on the input urban 3D model and meteorological data.

3. Results

Fig. 3a and Fig. 3b show the spatial distributions of LST and T_{mrt} in the city of Philadelphia on July 20th, 2019. Since the meteorological data that was used for urban microclimate modeling is only available every 30 min, therefore, T_{mrt} was calculated for 11:30 am (closest to Landsat overpass time at 11:39 am). In the LST map of July 20th (Fig. 3a), the LST distribution pattern aligns well with the distribution of tree canopies (Fig. 1). This is because the surface temperature of vegetation is lower than the surface temperature of developed land and impervious land (Paschalis et al., 2021). Water bodies also have much lower LST values than land pixels, but they are not a big presence in the city of Philadelphia. The LST map shows the general pattern of the heat distribution in the study area, while details of the temperature variance within neighborhoods are not clear due to the ~100 m resolution. Fig. 3b shows the spatial distribution of the T_{mrt} on July 20th at 11:30 am local time, and the water bodies pixels are not included. The T_{mrt} has a much higher spatial resolution (1 m) and presents a more detailed heat distribution across the study area (Fig. 3b). Similar to LST, T_{mrt} has a generally similar distribution with the tree canopy cover in Philadelphia. This is because tree canopies provide shade and help to lower the direct solar exposure on the ground. In the T_{mrt} map, the downtown areas have significant lower T_{mrt} values, because of the shade provided by the high-rise buildings (Fig. 3b). While in the LST map, such a pattern is not clear because the satellite view angle and the

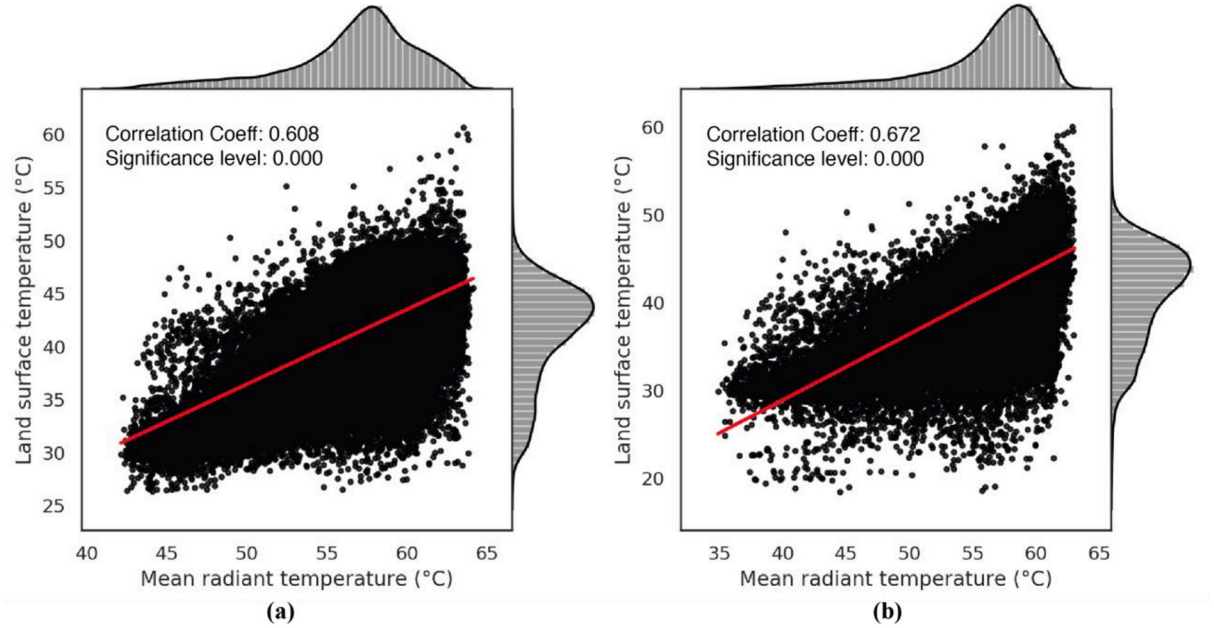

Fig. 4. The scatter plots of the mean radiant temperature (T_{mrt}) and the land surface temperature (LST) at the pixel level in the study area by resampling the T_{mrt} map to the same resolution as the LST, (a) the scatter plot of LST and T_{mrt} on July 20, 2019, (b) the scatter plot in the LST and T_{mrt} in the summertime from June to August of 2019.

resolution are insufficient to discern building shadows.

Fig. 3c shows the spatial distribution of the averaged LST from all available images (June 2nd, July 4th, July 20th, August 5th, August 21st) for summer 2019 after pixel-level quality-control for cloud contamination. The averaged LST map has a clearer spatial distribution of the LST than the LST map of July 20th in the study area. However, the spatial variations of the heat distribution across streets and neighborhoods are still not clear in the LST because of the coarse resolution. Fig. 3d shows the averaged T_{mrt} at 11:30 am local time for the same dates as the LST maps in order to make the data comparable. In the averaged T_{mrt} map, more heterogeneous heat distributions across neighborhoods and streets are seen.

In order to compare the LST and the T_{mrt} values, the 1 m T_{mrt} data were resampled to the same resolution as the Landsat LST using bilinear interpolation. Fig. 4 shows the scatter plots of the LST and T_{mrt} values for all non-water pixels in the city of Philadelphia for July 20, 2019 (Fig. 4a) and the summertime of 2019 (Fig. 4b). The T_{mrt} has a significant and positive correlation with the LST for both July 20th and the summertime of 2019 (Fig. 4). Although the T_{mrt} and LST have similar trend, T_{mrt} shows higher value than the LST for most pixels.

The Landsat-derived LST is not able to disentangle the surface temperature of different land use categories, while the high resolution T_{mrt} map reflects the different heat exposures on different land use types. On further examination, we compared the LST and T_{mrt} pixels overlaying different land use types. Fig. 5 shows the overlap of ~100 m LST pixel and the ~1 m T_{mrt} for building blocks, open space and road, forest, and grasslands in the study area. For each LST pixel, the T_{mrt} values were calculated as the mean values of all T_{mrt} pixels inside of the spatial extent of the LST pixels for each land use type. Fig. 6 shows the scatter plots of the summertime LST pixel values and the corresponding T_{mrt} values for buildings, open space and road, forest, and grass. For the developed land cover types based on NLCD (including land use types of building blocks, and open space and road), the LST value has a stronger correlation with T_{mrt} over the building block than over the open space and road (Table 1), which indicates the stronger relationship of LST with rooftop temperatures rather than roads. For the vegetated land cover types based on NLCD (including land use types of forest and grassland), the LST has a stronger correlation with T_{mrt} for the forest component than the grassland (Table 1).

Fig. 7 shows the spatio-temporal distribution of the T_{mrt} over time on July 20th, 2019. The T_{mrt} distribution changes significantly over time due to the different solar positions and the meteorological conditions. While the Landsat-derived LST data cannot indicate the temporal change of the surface temperature at details in the time other than the visiting time of the satellite.

4. Discussion

Extreme heat in urban areas is an increasingly dangerous threat to human well-being, particularly when exacerbated by global climate change. Quantitative understanding of the urban heat distribution is of great importance for monitoring heat vulnerability within cities, devising effective mitigation strategies, and ensuring climate resilience. This study, using the city of Philadelphia as a study area, investigated the comparability of satellite-derived LST, often used in multi-city studies to identify local urban warming and detect heat exposure hotspots, with T_{mrt}, a metric that provides a more physiologically relevant measure of heat exposure. Our findings

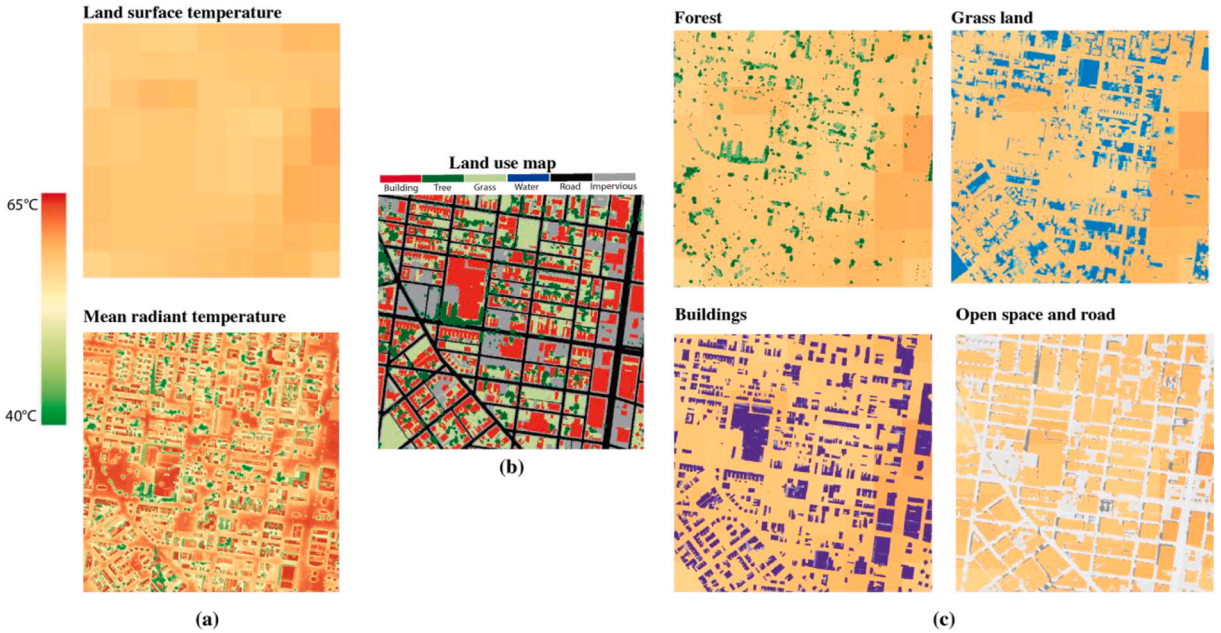

Fig. 5. The overlay of high resolution (1 m) mean radiant temperature (T_{mrt}) of different land use components on the coarse resolution (100 m) land surface temperature (LST), (a) the LST and T_{mrt} maps for a portion of the study area, (b) the land use map, (c) the overlay of T_{mrt} of different land use types on LST.

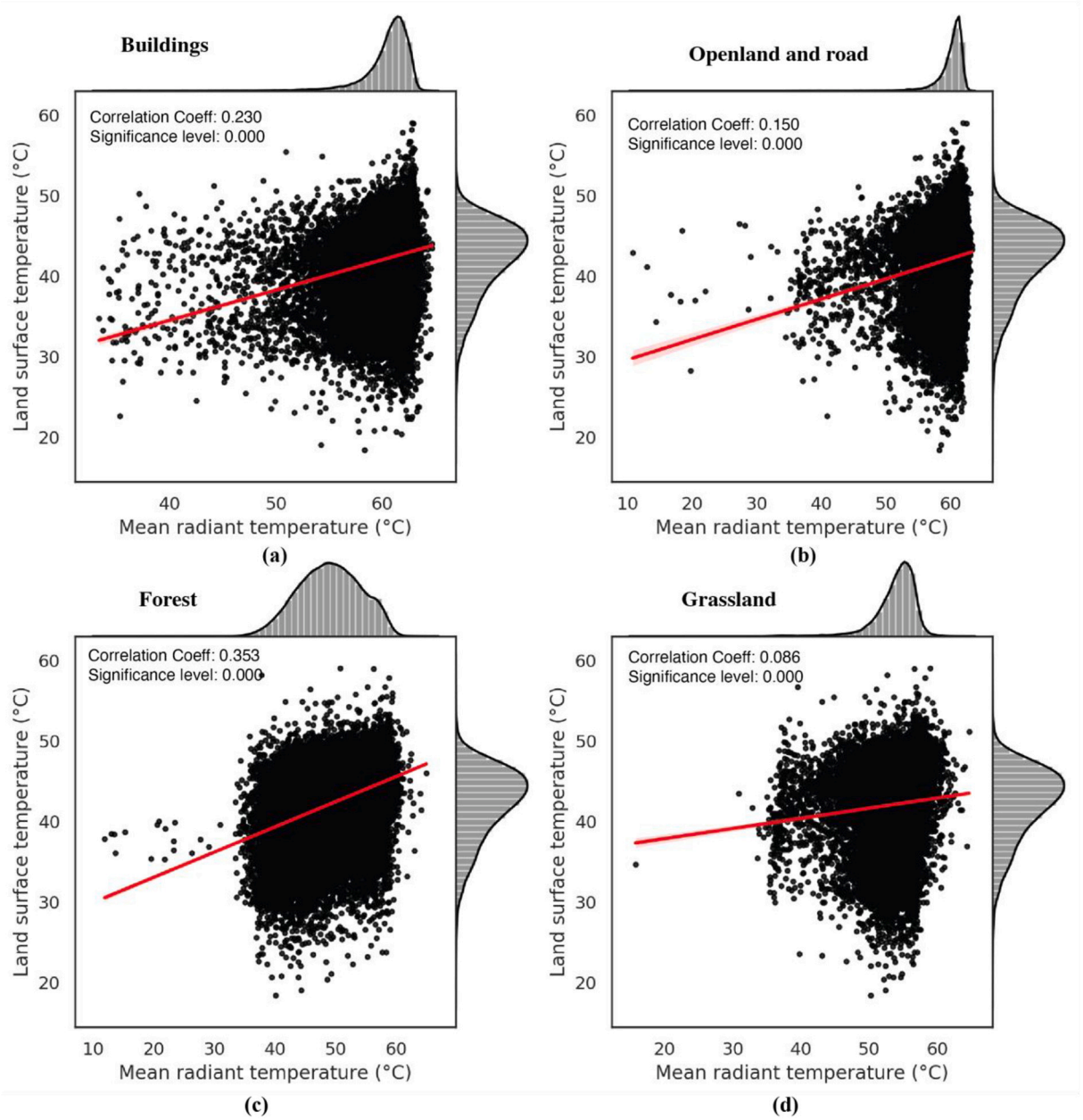

Fig. 6. The correlations of the LST and T_{mrt} components from building block, open space and road, forest, and grassland.

Table 1
The correlation coefficients between the land surface temperature (LST) and the mean radiant temperature (T_{mrt}) of different land use components for the study area.

Different land use components	Correlation coefficient	Significant level (N = 168,795)
Building blocks	0.230	0.000**
Open space and road	0.150	0.000**
Forest	0.353	0.000**
Grassland	0.086	0.000**

** Significant at the 0.01 level (2-tailed).

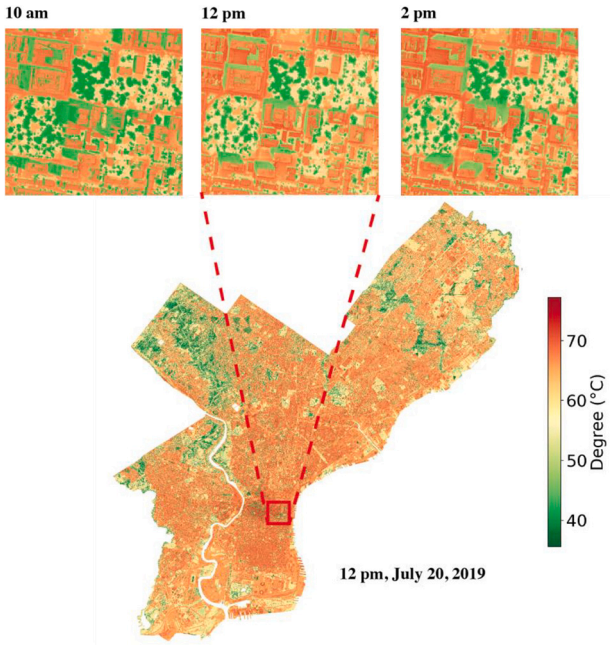

Fig. 7. The spatio-temporal distribution of T_{mrt} on July 20th, 2019 at different time points.

reveal a robust and statistically significant positive correlation LST and T_{mrt}, which indicates that both the LST and T_{mrt} can effectively present the overall distribution of urban heat across the city. The finer resolution T_{mrt} computed here provides more detailed information of the urban heat distribution with consideration of the impact of different urban landscape features, such as, street trees, building blocks, and other shading structures. This detailed information is crucial for identifying neighborhoods that are vulnerable to heat exposure (Li, 2021), which is also relevant for understanding heat-related environmental disparities in cities (Chakraborty et al., 2019; Hsu et al., 2021).

The study further disentangled the relationship between the Landsat-derived LST and modeled 1 m resolution T_{mrt} over different land use categories, such as building blocks, open space and road, forests, and grassland. Results show that the Landsat-derived LST has a stronger correlation with T_{mrt} over buildings than the open space and roads. However, it is important to note that building roofs are not directly relevant to pedestrian-scale thermal discomfort, and using the Landsat-derived LST cannot adequately capture outdoor heat exposure in densely built-up regions. Interestingly, LST and T_{mrt} over forests have a relatively strong correlation, suggesting similar variability of the top of the canopy temperature with the heat exposure below the tree canopies. While for the grassland, T_{mrt} has a relatively weak correlation with the LST, because the T_{mrt} on grassland is relatively high with no shade, but the surface temperature of grassland is generally cool.

Satellite observations of LST are constrained to the time of satellite overpass. However, the distribution of urban heat changes significantly over time, as seen from T_{mrt}. Thus, although more computationally expensive to generate, the high-temporal resolution T_{mrt} can provide more timely information of the dynamic changes in urban heat distribution throughout the day. The GPU-accelerated urban microclimate modeling is proved to be a highly efficient approach for generating city- and neighborhood-scale urban heat maps (Li and Wang, 2021). This methodology presents a powerful tool for understanding the dynamics of urban heat exposure in future studies. However, the modeling of T_{mrt} relies heavily on high-resolution spatial data as input. Developed countries benefit from robust data infrastructure and make it easy to generate such data. However, developing countries or regions lacking similar data infrastructure may face challenges in implementing this method. In areas where high resolution geospatial datasets are unavailable, the LST may still be a decent surrogate, especially when looking at the heat variability across the city.

The current study has several limitations that should be acknowledged. Firstly, we only examined the daytime urban outdoor heat exposure levels, and the nighttime heat exposure was not considered. This is because the Landsat LST is primarily captured during the daytime satellite overpass. However, nighttime and indoor heat exposure also impact human well-being. Previous studies show that the nighttime LST agrees well with the ambient air temperature (Zhang et al., 2014; Zhu et al., 2013). Therefore, using MODIS and ECOSTRESS LST may be able to estimate the ambient air temperature at nighttime, which can be further used as an input to estimate the T_{mrt} at night. Moreover, actual human heat exposure is also impacted significantly by adaptation as well as movement, clothing, use of parasols, etc., while these factors are not considered in this study.

This study only compared the medium-resolution Landsat-derived LST and T_{mrt} at different spatial and temporal resolution. Future studies should consider using higher-resolution LST for the comparison. Additionally, no field measurements were conducted to directly map actual human heat exposure in this study. Therefore, it is essential for future studies to incorporate ground measurements for further validation of the model. In the urban microclimate modeling, the albedo of the ground surface was assigned as a universal

value for each land use type, which does not consider the internal variations of albedo within the land use type. However, different pavement materials like concrete and asphalt may have very different reflectance of solar radiation. In future studies, a more detailed albedo map should be incorporated to better model the impact of the pavement types on human thermal comfort.

In addition, the T_{mrt} calculations also require fine temporal resolution meteorological data, such as air temperature, humidity, and radiation. In the present study, we used data from NREL, which cannot indicate the spatial variations throughout the city. Therefore, future studies should consider using finer level meteorological data to generate a smore objective method of the urban heat distribution at the city scale.

5. Conclusion

This study compared Landsat-derived land surface temperature (LST) and urban microclimate modeling-computed mean radiant temperature (T_{mrt}) for mapping urban-scale heat exposure distribution in Philadelphia. The fine resolution T_{mrt} is able to detect much more detailed information about urban heat with consideration of the fine level landscape factors, such as street trees, building blocks, etc. However, the T_{mrt} calculations require finer spatial resolution spatial data as input and are more computationally expensive to calculate, which limits the applicability of the method to those areas with good data infrastructure and computational resources. In contrast, the Landsat-derived LST can efficiently cover large areas. However, the coarse resolution LST is only able to show the general pattern of the urban heat distribution. It also cannot disentangle the heat contributions from different land use components, building roofs, top of tree canopies, grassland, and open land and road. The stronger correlation between LST and T_{mrt} on building roofs than the ground surface indicates that the coarse resolution LST may not provide a comprehensive understanding of pedestrian-level human heat exposure on the ground. In addition, the T_{mrt} can generate urban heat distribution at high temporal resolution, while the Landsat-derived LST is fixed to the satellite overpass times. This comparison provides a valuable reference for selecting more appropriate metrics in urban heat-related studies.

CRediT authorship contribution statement

Xiaojiang Li: Conceptualization, Methodology, Data curation, Writing – original draft. **Tirthankar Chakraborty:** Formal analysis, Writing – review & editing. **Guoqing Wang:** Formal analysis, Writing – review & editing.

Declaration of Competing Interest

This study has no conflict of interest. This project is supported by the National Science Foundation under Grant Number 2314709. We also thank Temple University High Performance Computing for providing support. T.C.'s contribution was supported by the Regional and Global Modeling and Analysis program area of the U.S. Department of Energy, Office of Science, Office of Biological and Environmental Research as part of the multi-program, collaborative Integrated Coastal Modeling (ICoM) project. PNNL is operated for DOE by Battelle Memorial Institute, United States under contract DE-AC05-76RL01830.

Data availability

Data will be made available on request.

References

Ali-Toudert, F., Mayer, H., 2006. Numerical study on the effects of aspect ratio and orientation of an urban street canyon on outdoor thermal comfort in hot and dry climate. Build. Environ. 41 (2), 94–108.

Aviv, D., Guo, H., Middel, A., Meggers, F., 2021. Evaluating radiant heat in an outdoor urban environment: resolving spatial and temporal variations with two sensing platforms and data-driven simulation. Urban Clim. 35, 100745.

Borden, K.A., Cutter, S.L., 2008. Spatial patterns of natural hazards mortality in the United States. Int. J. Health Geogr. 7 (1), 1.

Buo, I., Sagris, V., Jaagus, J., Middel, A., 2023. High-resolution thermal exposure and shade maps for cool corridor planning. Sustain. Cities Soc. 93, 104499.

Cao, J., Zhou, W., Zheng, Z., Ren, T., Wang, W., 2021. Within-city spatial and temporal heterogeneity of air temperature and its relationship with land surface temperature. Landsc. Urban Plan. 206, 103979.

Chakraborty, T., Hsu, A., Manya, D., Sheriff, G., 2019. Disproportionately higher exposure to urban heat in lower-income neighborhoods: a multi-city perspective. Environ. Res. Lett. 14 (10), 105003.

Chakraborty, T.C., Lee, X., Ermida, S., Zhan, W., 2021. On the land emissivity assumption and Landsat-derived surface urban heat islands: A global analysis. Remote Sens. Environ. 265, 112682.

Chakraborty, T., Venter, Z.S., Qian, Y., Lee, X., 2022. Lower urban humidity moderates outdoor heat stress. AGU Adv. 3 https://doi.org/10.1029/2022AV000729 e2022AV000729.

Chen, X.L., Zhao, H.M., Li, P.X., Yin, Z.Y., 2006. Remote sensing image-based analysis of the relationship between urban heat island and land use/cover changes. Remote Sens. Environ. 104 (2), 133–146.

Chen, L., Yu, B., Yang, F., Mayer, H., 2016. Intra-urban differences of mean radiant temperature in different urban settings in Shanghai and implications for heat stress under heat waves: A GIS-based approach. Energ. Build. 130, 829–842.

Gabriel, K.M.A., Endlicher, W.R., 2011. Urban and rural mortality rates during heat waves in Berlin and Brandenburg, Germany. Environ. Pollut. 159 (8–9), 2044–2050.

Gál, C.V., Kántor, N., 2020. Modeling mean radiant temperature in outdoor spaces, A comparative numerical simulation and validation study. Urban Clim. 32, 100571.

Hammer, J., Ruggieri, D.G., Thomas, C., Caum, J., 2020. Local extreme heat planning: an interactive tool to examine a heat vulnerability index for Philadelphia, Pennsylvania. J. Urban Health 97 (4), 519–528.

Harlan, S.L., Declet-Barreto, J.H., Stefanov, W.L., Petitti, D.B., 2013. Neighborhood effects on heat deaths: social and environmental predictors of vulnerability in Maricopa County, Arizona. Environ. Health Perspect. 121 (2), 197–204.
Ho, H.C., Wong, M.S., 2019. Urban environmental influences on the temperature–mortality relationship associated mental disorders and cardiorespiratory diseases during normal summer days in a subtropical city. Environ. Sci. Pollut. Res. 26 (23), 24272–24285.
Hsu, A., Sheriff, G., Chakraborty, T., Manya, D., 2021. Disproportionate exposure to urban heat island intensity across major US cities. Nat. Commun. 12 (1), 1–11.
Hulley, G.C., Hook, S.J., Abbott, E., Malakar, N., Islam, T., Abrams, M., 2015. The ASTER global emissivity dataset (ASTER GED): mapping Earth's emissivity at 100 meter spatial scale. Geophys. Res. Lett. 42 (19), 7966–7976.
Jenerette, G.D., Harlan, S.L., Buyantuev, A., Stefanov, W.L., Declet-Barreto, J., Ruddell, B.L., Li, X., 2016. Micro-scale urban surface temperatures are related to land-cover features and residential heat related health impacts in Phoenix, AZ USA. Landsc. Ecol. 31 (4), 745–760.
Kianmehr, A., Lim, T.C., Li, X., 2023. Comparison of different spatial temperature data sources and resolutions for use in understanding intra-urban heat variation. Sustain. Cities Soc. 96, 104619.
Klemm, W., Heusinkveld, B.G., Lenzholzer, S., van Hove, B., 2015. Street greenery and its physical and psychological impact on thermal comfort. Landsc. Urban Plan. 138, 87–98.
Kong, F., Chen, J., Middel, A., Yin, H., Li, M., Sun, T., Ma, J., 2022. Impact of 3-D urban landscape patterns on the outdoor thermal environment: A modelling study with SOLWEIG. Comput. Environ. Urban. Syst. 94, 101773.
Laaidi, K., Zeghnoun, A., Dousset, B., Bretin, P., Vandentorren, S., Giraudet, E., Beaudeau, P., 2012. The impact of heat islands on mortality in Paris during the august 2003 heat wave. Environ. Health Perspect. 120 (2), 254–259.
Lee, H., Holst, J., Mayer, H., 2013. Modification of human-biometeorologically significant radiant flux densities by shading as local method to mitigate heat stress in summer within urban street canyons. Adv. Meteorol. 2013.
Li, X., 2021. Investigating the spatial distribution of resident's outdoor heat exposure across neighborhoods of Philadelphia, Pennsylvania using urban microclimate modeling. Sustain. Cities Soc. 103066.
Li, X., Wang, G., 2021. GPU parallel computing for mapping urban outdoor heat exposure. Theor. Appl. Climatol. 1–11.
Lin, S., Hsu, W.H., Van Zutphen, A.R., Saha, S., Luber, G., Hwang, S.A., 2012. Excessive heat and respiratory hospitalizations in New York state: estimating current and future public health burden related to climate change. Environ. Health Perspect. 120 (11), 1571–1577.
Lindberg, F., Grimmond, C.S.B., 2011. The influence of vegetation and building morphology on shadow patterns and mean radiant temperature in urban areas: model development and evaluation. Theor. Appl. Climatol. 105 (3), 311–323.
Lindberg, F., Holmer, B., Thorsson, S., 2008. SOLWEIG 1.0–modelling spatial variations of 3D radiant fluxes and mean radiant temperature in complex urban settings. Int. J. Biometeorol. 52 (7), 697–713.
Lindberg, F., Grimmond, C.S.B., Gabey, A., Huang, B., Kent, C.W., Sun, T., Zhang, Z., 2018. Urban multi-scale environmental predictor (UMEP): an integrated tool for city-based climate services. Environ. Model. Softw. 99, 70–87.
Luber, G., McGeehin, M., 2008. Climate change and extreme heat events. Am. J. Prev. Med. 35 (5), 429–435.
Maronga, B., Gryschka, M., Heinze, R., Hoffmann, F., Kanani-Sühring, F., Keck, M., Raasch, S., 2015. The parallelized large-Eddy simulation model (PALM) version 4.0 for atmospheric and oceanic flows: model formulation, recent developments, and future perspectives. Geosci. Model Dev. 8 (8), 2515–2551.
Matzarakis, A., Rutz, F., Mayer, H., 2007. Modelling radiation fluxes in simple and complex environments—application of the RayMan model. Int. J. Biometeorol. 51 (4), 323–334.
Matzarakis, A., Rutz, F., Mayer, H., 2010. Modelling radiation fluxes in simple and complex environments: basics of the RayMan model. Int. J. Biometeorol. 54 (2), 131–139.
Mayer, H., Höppe, P., 1987. Thermal comfort of man in different urban environments. Theor. Appl. Climatol. 38 (1), 43–49.
Middel, A., Krayenhoff, E.S., 2019. Micrometeorological determinants of pedestrian thermal exposure during record-breaking heat in Tempe, Arizona: introducing the MaRTy observational platform. Sci. Total Environ. 687, 137–151.
Mutiibwa, D., Strachan, S., Albright, T., 2015. Land surface temperature and surface air temperature in complex terrain. IEEE J. Select. Top. Appl. Earth Observat. Remote Sens. 8 (10), 4762–4774.
Noelke, C., McGovern, M., Corsi, D.J., Jimenez, M.P., Stern, A., Wing, I.S., Berkman, L., 2016. Increasing ambient temperature reduces emotional well-being. Environ. Res. 151, 124–129.
Norton, B.A., Coutts, A.M., Livesley, S.J., Harris, R.J., Hunter, A.M., Williams, N.S., 2015. Planning for cooler cities: A framework to prioritise green infrastructure to mitigate high temperatures in urban landscapes. Landsc. Urban Plan. 134, 127–138.
Paschalis, A., Chakraborty, T.C., Fatichi, S., Meili, N., Manoli, G., 2021. Urban forests as main regulator of the evaporative cooling effect in cities. AGU Adv. 2 (2) e2020AV000303.
Pearsall, H., 2017. Staying cool in the compact city: vacant land and urban heating in Philadelphia, Pennsylvania. Appl. Geogr. 79, 84–92.
Reid, C.E., O'neill, M.S., Gronlund, C.J., Brines, S.J., Brown, D.G., Diez-Roux, A.V., Schwartz, J., 2009. Mapping community determinants of heat vulnerability. Environ. Health Perspect. 117 (11), 1730–1736.
Sekertekin, A., Bonafoni, S., 2020. Land surface temperature retrieval from Landsat 5, 7, and 8 over rural areas: assessment of different retrieval algorithms and emissivity models and toolbox implementation. Remote Sens. 12 (2), 294.
Stone, B., Hess, J.J., Frumkin, H., 2010. Urban form and extreme heat events: are sprawling cities more vulnerable to climate change than compact cities? Environ. Health Perspect. 118 (10), 1425–1428.
Thorsson, S., Rocklöv, J., Konarska, J., Lindberg, F., Holmer, B., Dousset, B., Rayner, D., 2014. Mean radiant temperature–A predictor of heat related mortality. Urban Clim. 10, 332–345.
Vancutsem, C., Ceccato, P., Dinku, T., Connor, S.J., 2010. Evaluation of MODIS land surface temperature data to estimate air temperature in different ecosystems over Africa. Remote Sens. Environ. 114 (2), 449–465.
Vanos, J.K., Warland, J.S., Gillespie, T.J., Slater, G.A., Brown, R.D., Kenny, N.A., 2012. Human energy budget modeling in urban parks in Toronto and applications to emergency heat stress preparedness. J. Appl. Meteorol. Climatol. 51 (9), 1639–1653.
Venter, Z.S., Chakraborty, T., Lee, X., 2021. Crowdsourced air temperatures contrast satellite measures of the urban heat island and its mechanisms. Sci. Adv. 7 (22), eabb9569.
Wang, C., Zhang, Z., Zhou, M., Wang, P., Yin, P., Ye, W., Zhang, L., 2018. Different response of human mortality to extreme temperatures (MoET) between rural and urban areas: a multi-scale study across China. Health Place 50, 119–129.
Watts, N., Adger, W.N., Agnolucci, P., Blackstock, J., Byass, P., Cai, W., Costello, A., 2015. Health and climate change: policy responses to protect public health. Lancet 386 (10006), 1861–1914.
Weber, S., Sadoff, N., Zell, E., de Sherbinin, A., 2015. Policy-relevant indicators for mapping the vulnerability of urban populations to extreme heat events: A case study of Philadelphia. Appl. Geogr. 63, 231–243.
Yu, Q., Ji, W., Pu, R., Landry, S., Acheampong, M., O'Neil-Dunne, J., Tanim, S.H., 2020. A preliminary exploration of the cooling effect of tree shade in urban landscapes. Int. J. Appl. Earth Obs. Geoinf. 92, 102161.
Zhang, P., Bounoua, L., Imhoff, M.L., Wolfe, R.E., Thome, K., 2014. Comparison of MODIS land surface temperature and air temperature over the continental USA meteorological stations. Can. J. Remote. Sens. 40 (2), 110–122.
Zhu, W., Lű, A., Jia, S., 2013. Estimation of daily maximum and minimum air temperature using MODIS land surface temperature products. Remote Sens. Environ. 130, 62–73.